Supplementary Information

Experimental

Materials and Electrochemistry

The same X-ray transparent *in situ* pouch cell design and sample holder plates were used for both 2D and 3D imaging,[1] although the imaging holes in the plates were enlarged horizontally to allow imaging at high tilt angles of the sample with respect to the X-ray beam (3D). The pouch cells comprised of a lithium metal counter/reference electrode, Celgard separator soaked in 1.0 M $LiPF_6$ in 1:1 w/w ethylene carbonate/diethyl carbonate electrolyte (BASF), and a working electrode composed of micron-sized Ge particles (45 wt%, Aldrich), Super P carbon (45 wt%), and PVDF binder (10 wt%) slurry-coated on a 2.5 μm ultrathin nickel foil (Alfa Aesar). The ultrathin Ni foil is sufficiently transparent to 11.2 keV x-rays at high tilt angle (~70˚). The working electrode was roll-pressed before cell assembly. The Ge particle loading (~0.2 mg cm^{-2}) was chosen such that a set of particles could be tracked at each angle as the cell was rotated through an angular range of approximately 140˚.

The cells were cycled using a MTI eight-channel analyzer (0.02 – 1 mA) at a constant rate of C/5 based on the theoretical capacity of Ge (1600 mAh g^{-1}). A cycling current of C/*x* is calculated such that a single half cycle (lithiation or delithiation) will require theoretically *x* hours to complete. The potential window was 2.0 V to 0.0 V *vs.* Li/Li^+. Because of the higher than typical carbon loading, the total cell capacities slightly exceeded the theoretical as lithium was inserted into the carbon.

Transmission X-ray Microscopy

X-ray images were recorded with 11.2 keV x-rays using the full field transmission X-ray microscope on beamline 6-2 at SLAC National Accelerator Laboratory's Stanford Synchrotron Radiation Lightsource (SSRL). The energy was chosen to maximize the Ge contrast with respect to the remaining battery components. The spatial resolution of this microscope is as fine as 30 nm in 2D and approximately 50 nm in 3D. The field of view for a single exposure at 11.2 keV is around 45 μm. Additional details on the microscope are found in papers by Andrews *et al.*,[2] Liu *et al.*, [3] and Meirer *et al.*.[4]

For *operando* 2D imaging, the cell was cycled concurrent with imaging. A total of five regions within the same cell were imaged approximately every 12 minutes. At each region two one-second images were recorded and averaged to improve the signal to noise ratio. A camera binning of two was used to further improve the image quality without increasing the dose to the sample. With this binning and X-ray energy, the pixel size of the 2D images is 44 nm.

Data Analysis

The average optical density (OD) of nine particles in five different imaging regions were calculated by thresholding the 2D images to create a binary mask of the particles. The mask was used to determine which pixels were contained within a particular particle. The average optical density (or absorption) for each particle was calculated by averaging the value of all pixels within the particle in the absorption images. By plotting the OD over the cycle, the potential at which the average OD initially dropped and then continued its downward trend was determined.

For *in situ* tomographic imaging, three regions within the same cell were each imaged in their fresh, lithiated, and delithiated states. The TXM setup is capable of *operando* tomographic imaging; however, it was found that such continuous imaging exceeds the total acceptable X-ray dose tolerated by the cell. Radiation damage, presumably to the electrolyte, renders the local imaging region inactive although the bulk of the battery continues to function normally. To mitigate damage from *operando* 3D imaging, fewer angular points have to be used. At each of the three regions a single two second image was recorded at each degree over a complete angular range of 140˚ - 142˚ depending on the region. A camera binning of one was used, resulting in a voxel size of 22 nm.

To quantify the density changes due to (de)lithiation in the reconstructed tomography data, the regions were individually normalized. For each region, two 100 x 100 x 100 voxel (2.2 μm x 2.2 μm x 2.2 μm) subvolumes were chosen in the before cycled state. One subvolume contained only background voxels while the second contained only voxels entirely within a Ge particle (Fig. S6). The histogram for each subvolume was fit with a Gaussian. The center position of the Gaussian peak was used either as the value for the background or as the value for pure Ge. All the voxels in the region in the three electrochemical states (before cycling, lithiated,

delithiated) we linearly normalized such that the background was zero density and pure Ge was the density of Ge (5.323 cm/g^{-3}). The average densities were calculated by fitting the histogram peaks from identically sized subvolumes within the same Ge particle in each electrochemical state.

X-ray micrographs were processed using TXM Wizard.[5] Analysis for the 2D imaging included reference correction and alignment of sequential images using a cross correlation algorithm. Analysis for the 3D imaging included reference correction, manual alignment of projection images, and tomographic reconstruction using the Algebraic Reconstruction Technique (ART) algorithm. For display purposes only, the tomographic reconstructions were smoothed with a median filter to reduce the visibility of high frequency artifacts that stem from the missing angular data. All calculations were performed on unsmoothed data. Visualization, median filtering, and density calculations of the 3D reconstructions were performed using the Avizo Fire software package. Area determination and optical density calculations on the 2D images were completed using ImageJ software.

References

1. J. Nelson, S. Misra, Y. Yang, A. Jackson, Y. Liu, H. Wang, H. Dai, J. C. Andrews, Y. Cui and M. F. Toney, *Journal of American Chemical Society*, 2012, 134, 6337-6343.
2. J. C. Andrews, E. Almeida, M. C. van der Meulen, J. S. Alwood, C. Lee, Y. Liu, J. Chen, F. Meirer, M. Feser, J. Gelb, J. Rudati, A. Tkachuk, W. Yun and P. Pianetta, *Microscopy and microanalysis : the official journal of Microscopy Society of America, Microbeam Analysis Society, Microscopical Society of Canada*, 2010, 16, 327-336.
3. Y. Liu, J. C. Andrews, J. Wang, F. Meirer, P. Zhu, Z. Wu and P. Pianetta, *Opt. Express*, 2011, 19, 540-545.
4. F. Meirer, J. Cabana, Y. Liu, A. Mehta, J. C. Andrews and P. Pianetta, *Journal of synchrotron radiation*, 2011, 18, 773-781.
5. Y. Liu, F. Meirer, P. A. Williams, J. Wang, J. C. Andrews and P. Pianetta, *Journal of synchrotron radiation*, 2012, 19, 281-287.

M1. Movie of *in situ* TXM absorption snapshots of micron-size germanium particles during first and second cycle for the region shown in Figures 1 and S1. The voltages at which the images were recorded are given in the top left corner. Because the images are displayed on the same contrast and brightness scale and we can assume there is negligible absorption contribution from lithium, then any changes in brightness is linearly proportional to a change in particle density. Images were taking at 11.2 keV with a pixel size of 44 nm.

M2. Movie of *in situ* TXM absorption snapshots of micron-size germanium particles during first and second cycle for the region shown in Figure S3. The voltages at which the images were recorded are given in the top left corner. Because the images are displayed on the same contrast and brightness scale and we can assume there is negligible absorption contribution from lithium, then any changes in brightness is linearly proportional to a change in particle density. Images were taking at 11.2 keV with a pixel size of 44 nm.

M3. Movie of *in situ* TXM absorption snapshots of micron-size germanium particles during first and second cycle. Note that only the upper large particle shows volume changes during the second cycle. The voltages at which the images were recorded are given in the top left corner. Because the images are displayed on the same contrast and brightness scale and we can assume there is negligible absorption contribution from lithium, then any changes in brightness is linearly proportional to a change in particle density. Images were taking at 11.2 keV with a pixel size of 44 nm.

M4. Movie of *in situ* TXM absorption snapshots of micron-size germanium particles during first and second cycle. Note that none of the particles show volume changes during the second cycle. The voltages at which the images were recorded are given in the top left corner. Because the images are displayed on the same contrast and brightness scale and we can assume there is negligible absorption contribution from lithium, then any changes in brightness is linearly proportional to a change in particle density. Images were taking at 11.2 keV with a pixel size of 44 nm.

M5. Movie of *in situ* TXM absorption snapshots of micron-size germanium particles during first and second cycle. Note that none of the particles show volume changes during the second cycle. The voltages at which the images were recorded are given in the top left corner. Because the images are displayed on the same contrast and brightness scale and we can assume there is negligible absorption contribution from lithium, then any changes in brightness is linearly proportional to a change in particle density. Images were taking at 11.2 keV with a pixel size of 44 nm.

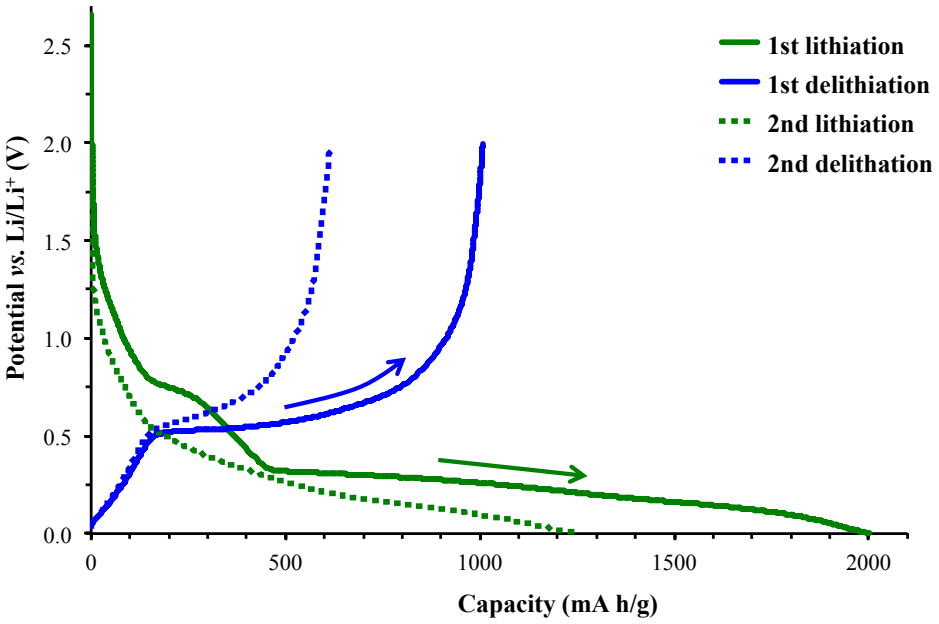

Figure S1. Voltage capacity plot of the first and second lithiation/delithiation during *in operando* TXM imaging. There is a 37% drop in capacity between the first and second lithiation cycles.

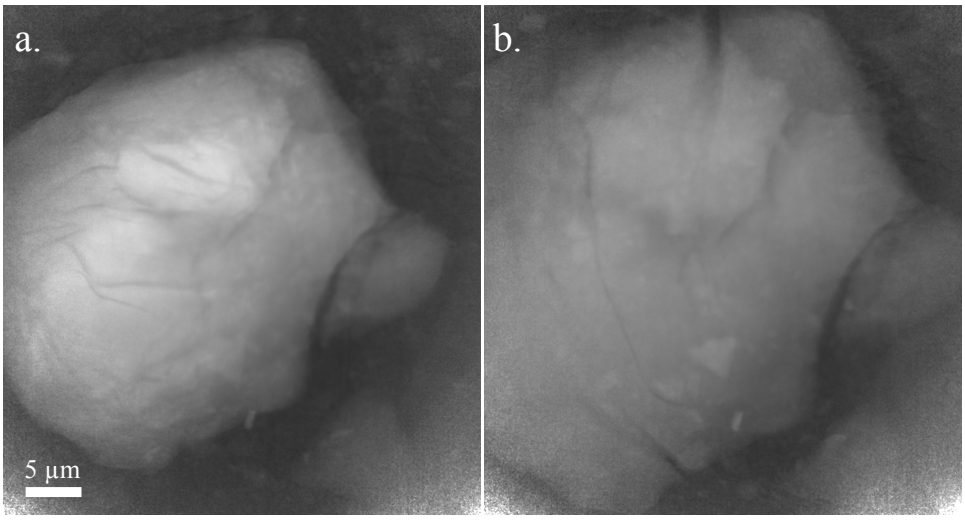

Figure S2. *In situ* TXM absorption snapshots of the largest particle observed after the first lithation cycle (a) and after the second lithation cycle (b). The volume expansion is significantly larger during the second lithiation cycle.

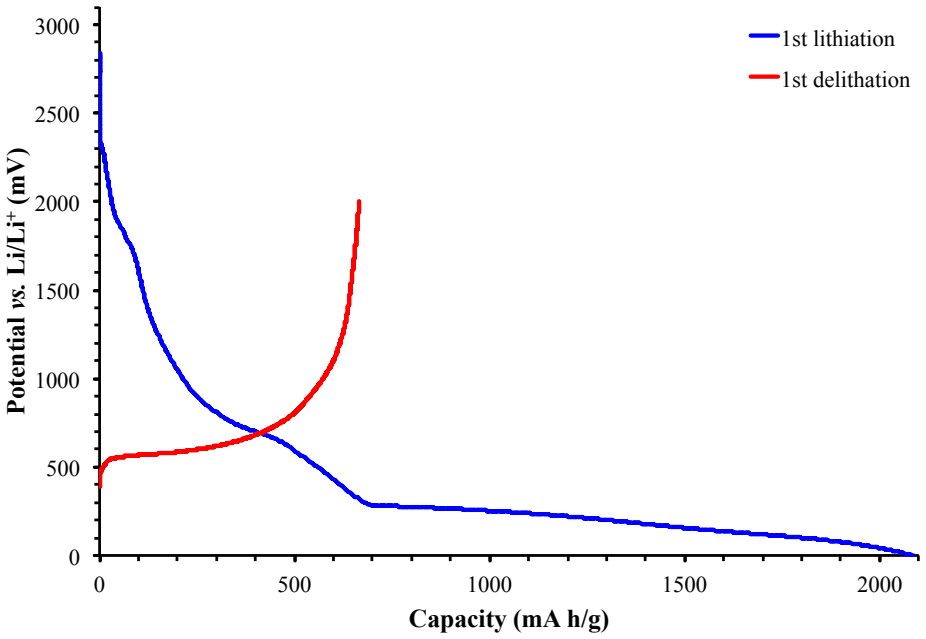

Figure S3. Electrochemistry of first lithiation and delithiation cycles of the *in situ* tomography cell.

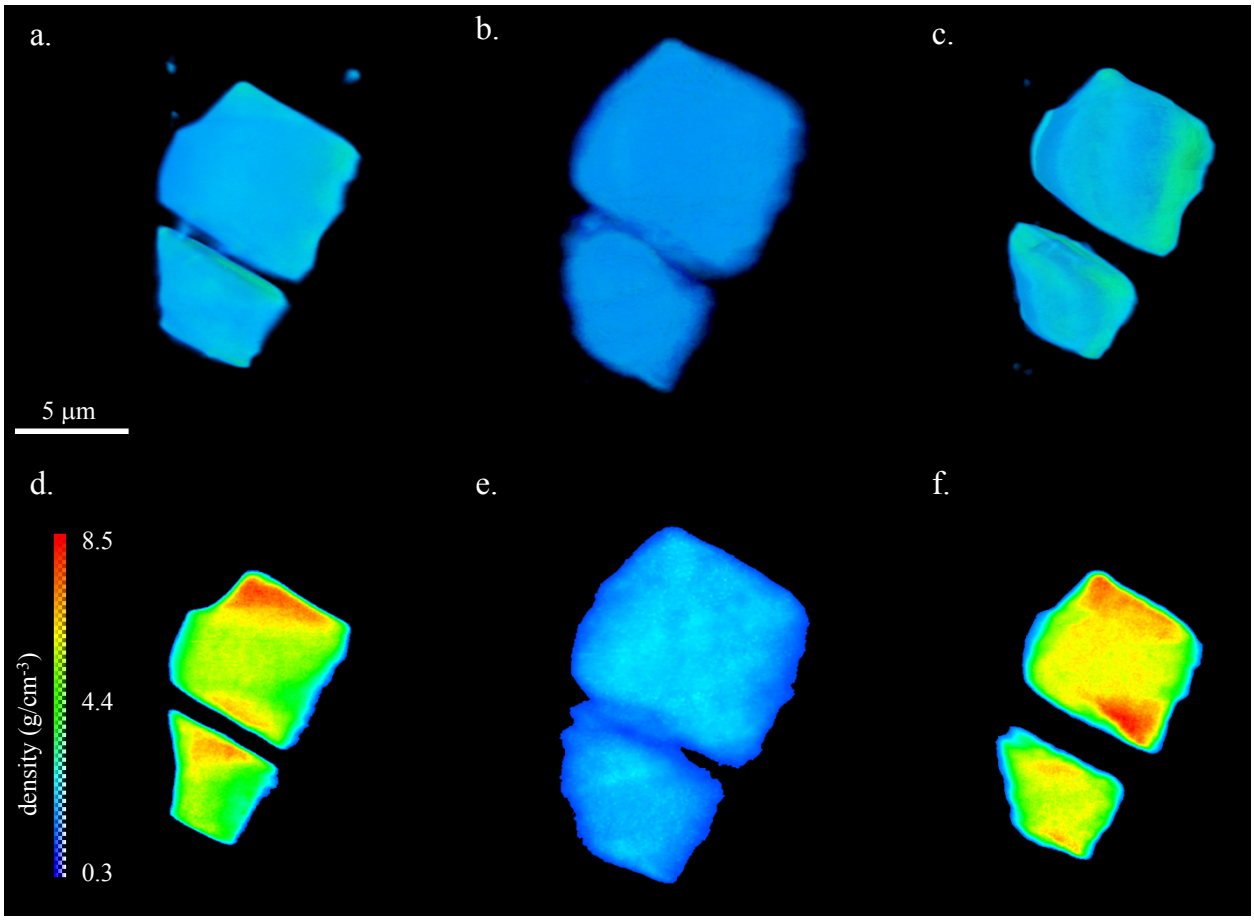

Figure S4. Volume renderings with corresponding cross-sections through the volume from *in situ* tomographic imaging of Ge particles (a, d) before cycling, (b, e) after the first lithiation cycle, and (c, f) after the first delithiation cycle. To reduce the visibility of sharp features that are artifacts stemming from the missing angular data, the tomographic data were smoothed with a median filter for display purposes. The scale and color bars correspond to the volume renderings and 2D slices.

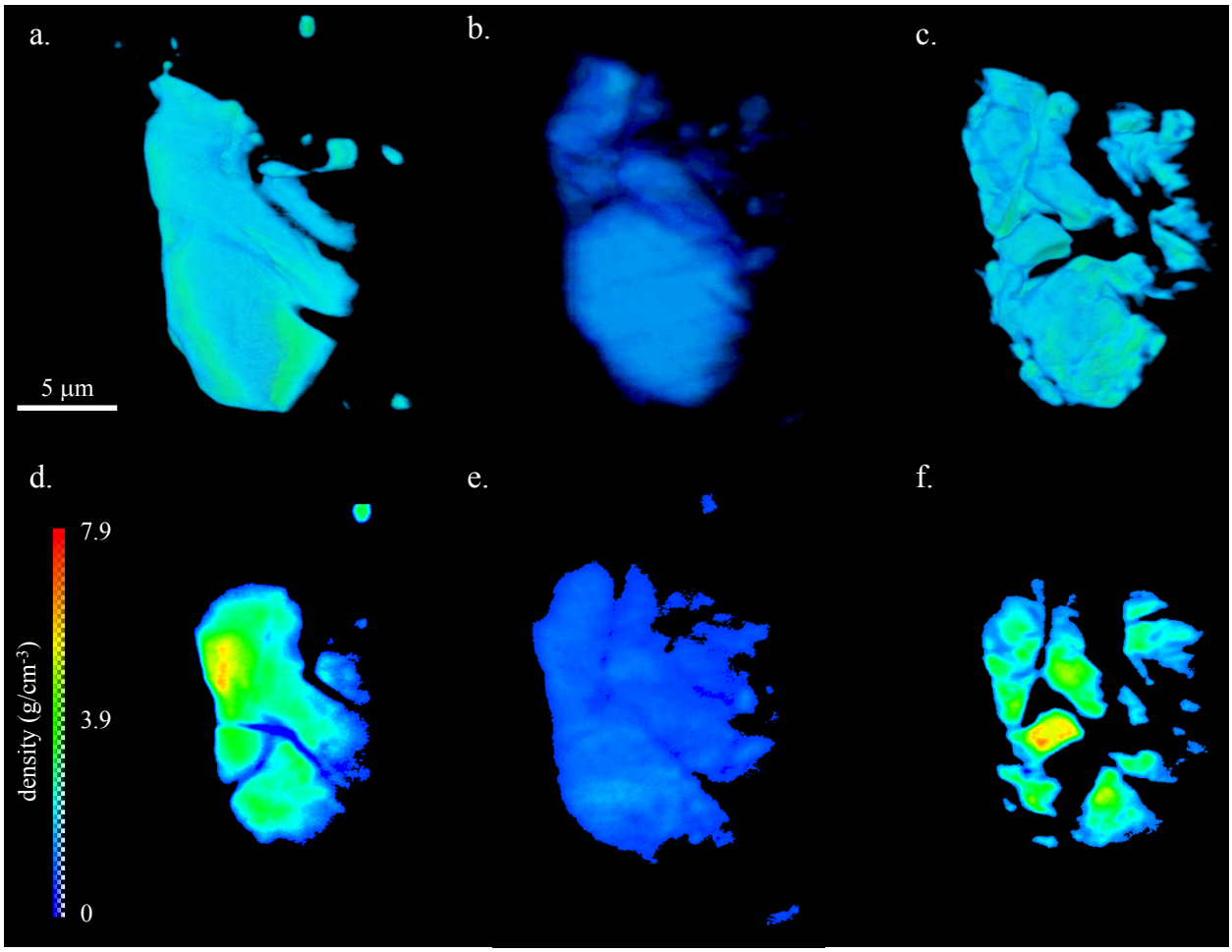

Figure S5. Volume renderings (above) with corresponding cross-sections through the volume (below) from *in situ* tomographic imaging of Ge particles (a, d) before cycling, (b, e) after the first lithiation cycle, and (c, f) after the first delithiation cycle. Data were smoothed with a median filter for display purposes to reduce the visibility of sharp features that are artifacts stemming from the missing angular data. The scale bar corresponds to the volume renderings and 2D slices.

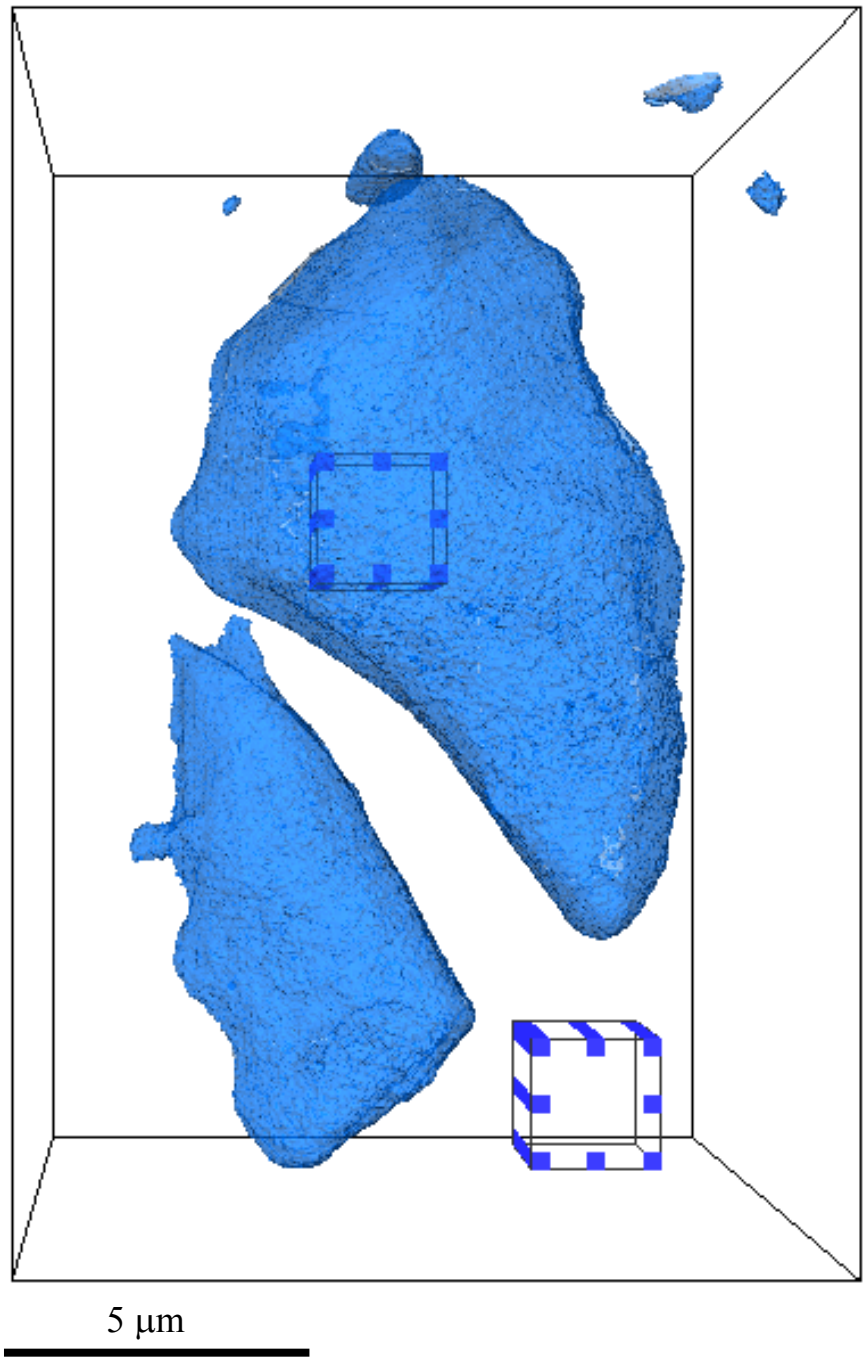

Figure S6. Surface rendering of Ge particles before cycling from Fig. 5 with 2.2 µm x 2.2 µm x 2.2 µm subvolumes containing either only voxels entirely within a Ge particle (upper) or only background voxels (lower). These subvolumes are used to normalize the voxel intensities as described in the Methods Section.